Article

Off-resonant absorption enhancement in single nanowires via graded dual-shell design

Wenfu Liu [1,2*], Xiaolei Guo [1], Shule Xing [1], Haizi Yao [1], Yinling Wang [1], Liuyang Bai [1], Qi Wang [1], Liang Zhang [1], Dachuan Wu [2], Yuxiao Zhang [2], Xiao Wang [2] and Yasha Yi [2,3*]

[1] School of Mechanical and Energy Engineering, Huanghuai University, Zhumadian, Henan 463000, China; liuwenfu@huanghuai.edu.cn (W.L.); guoxiaolei@huanghuai.edu.cn (X.G.); xingshule@huanghuai.edu.cn (S.X.); yaohaizi@huanghuai.edu.cn (H.Y.); wangyinlin@huanghuai.edu.cn (Y.W.); bailiuyang@huanghuai.edu.cn (L.B.); wangqi@huanghuai.edu.cn (Q.W.); zhangliang@huanghuai.edu.cn (L.Z.)

[2] Integrated Nano Optoelectronics Laboratory, University of Michigan, Dearborn, MI 48128, USA; dachuanw@umich.edu (D.W.); yuxiaoz@umich.edu (Y. Z.); xwa@umich.edu (X. W.); yashayi@umich.edu (Y.Y.)

[3] Energy Institute, University of Michigan, Ann Arbor, MI 48109, USA; yashayi@umich.edu (Y.Y.)

* Correspondence: liuwenfu@huanghuai.edu.cn (W.L.); yashayi@umich.edu (Y.Y.)

Abstract: Single nanowires (NWs) are of great importance for various optoelectronic applications, especially solar cells serving as powering nanoscale devices. However, weak off-resonant absorption can limit its light-harvesting capability. Here, we propose a single NW coated with the graded-index dual shells (DSNW). We demonstrate that with the proper thickness and refractive index of the inner shell, the DSNW exhibits significantly enhanced light trapping compared with the bare NW (BNW), and the NW only coated with the outer shell (OSNW) and inner shell (ISNW), which can be attributed to the optimal off-resonant absorption mode profiles due to the improved coupling between the reemitted light of the leak mode resonances of the Si core and the nanofocusing light from the dual shells with the graded refractive index. We found that the light absorption can be adjusted via tuning the thickness and refractive index of the inner shell, the photocurrent density is significantly enhanced by 134% (56%, 12%) in comparison with that of the BNW (OSNW, ISNW). This work advances our understanding of how to improve off-resonant absorption by applying graded dual shells and provides a new choice for designing high-efficiency single NW photovoltaic devices.

Keywords: single nanowires; Silicon; dual shells; off-resonance; absorption; photocurrent

---

1. Introduction

Single nanowire (NW) solar cells have attracted more and more research interests as nanoelectronic power sources in recent years due to their unique characteristics, such as enhanced light-harvesting capability, efficient carrier collection, ultra-compact volume, large surface area, and convenience of integrating with optoelectronic nanosystems [1-8]. Moreover, the design at the single level is of great importance to understand optoelectronic characteristics of the assembled NWs and thus can simplify analysis to obtain the theoretical limits for photovoltaic applications [7-14]. It is well known that light-harvesting ability is one of the most critical factors for photovoltaic applications, which determines the photoelectric conversion efficiency of a solar cell. Surprisingly, there is a strong interaction of the incident light with a single NW, which leads to a much higher absorption cross-section than its physical geometry [15-17]. However, the light absorption of single NWs is still far from the expectation due to the sharp optical resonant peak and narrow width, which can only achieve superior light absorption at the peak position.

Preprints (www.preprints.org) | NOT PEER-REVIEWED | Posted: 11 August 2020 doi:10.20944/preprints202008.0258.v1

Therefore, various strategies have been implemented to improve the light absorption in the whole solar spectrum range. It was shown that the light absorption could be readily tuned by controlling the size, geometry, and orientation of the NWs [18-26]. Moreover, our previous studies [27,28] showed that the light absorption could be further improved by introducing a non-absorbing dielectric shell as the antireflection coating, which was experimentally and numerically demonstrated in the recent studies [29-33]. Comparing to the bare NWs (BNWs), semiconductor core-dielectric shell NWs (CSNWs) not only provides the possibility to tune the position of the resonant peak but also enhance the light-harvesting capability in the off-resonant region by adjusting the thickness and complex refractive index of the shell, which is attributed to the high nanofocusing effect [27,33]. However, a further increase of the shell thickness has little contribution to the enhancement of the light absorption of the CSNW structure because the incident light will be mainly concentrated in the dielectric shell. Recently, some new strategies have been employed to improve the light-trapping capability of the CSNW, including the off-axial core-shell [34], and partially capped design [35]. At the same time, the graded-index concept has been employed to enhance light absorption in the two-dimensional structures [36-38]. However, to our knowledge, the dual shells with the graded refractive index have not been applied to improve the light absorption of single NWs.

In this work, we report a single dual-shell coated NW (DSNW), in which the dual shells have a graded refractive index. Graded dual-shell design leads to dramatically improved off-resonant absorption. The detailed analysis of the absorption mode and generation rate profiles shows that this enhancement results mainly from the leaky mode resonances (LMRs) under an improved coupling between the reemitted light of the leak mode resonances of the Si core and the nanofocusing light from the dual shells with the graded refractive index. Simulation results indicate that the photocurrent density is significantly enhanced by 134%, 56%, and 12% in comparison with that of the BNW, and the nanowire only coated with the outer shell (OSNW) and inner shell (ISNW), respectively.

2. Model and Methods

2.1. Model

The cross-sectional schematic diagram of the DSNW is shown in the insets of Figure 1. It should be noted here that the OSNW and ISNW are also shown for comparison. The geometrical parameters of the DSNW are characterized by the radius r (=100 nm) of Si core, the thickness t_1 of the outer shell and the thickness t_2 of the inner shell of the DSNW which varies from t_2=0 nm (i.e., OSNW) to t_2=180 nm (i.e., ISNW), the total shell thickness $t=t_1+t_2$=180 nm, and the total radius $R=r+t$=280 nm. The incident light indicated by colorful arrows in the insets of Figure 1 is assumed to be illuminated perpendicularly to the axial from the top, the wavelength range is from 300 to 1100 nm with a step size of 5 nm considering solar radiation and the bandgap of Si. The wavelength-dependent complex refractive index of Si fitted with the experimental data [39], and that of the inner shell (close to Si_3N_4), the outer shell (close to SiO_2), and the surrounding medium (air) are set to be 2.5, 1.5, and 1.0, respectively.

2.2. Methods

The light absorption performance of the DSNW was performed by solving the corresponding Maxwell's equations based on the two-dimensional (2D) finite difference time domain (FDTD) method [40-42] by assuming that the length of the NW is far greater than the radius, which can be referred to the work of Kim and co-workers for details [24-26,31]. In this simulation, the perfectly matched layers (PML) boundary conditions are used to avoid any non-physical reflection with the boundaries, the total-field scattered-field (TFSF) method was applied to ensure that a single NW interacts with an infinite plane wave. Also, the minimum cell size of the FDTD mesh is set to 1 nm to guarantee the accuracy of the simulation results.

2.2.1. The absorption efficiency and mode profile

Preprints (www.preprints.org) | NOT PEER-REVIEWED | Posted: 11 August 2020 doi:10.20944/preprints202008.0258.v1

To qualify the light absorption performance of the DSNW, we define the absorption efficiency Q_{abs} of the Si core as [33,43-45]:

$$Q_{abs} = C_{abs}/C_{geo} \tag{1}$$

where C_{geo} is the geometric cross-section (i.e., the projected area of the Si core), and C_{abs} is the absorption cross-section calculated by [33,43-45]

$$C_{abs} = \frac{\int_V P_{abs} dV}{I_0} = k_0 \varepsilon_r'' \int_V |E_r|^2 \, dV \tag{2}$$

where k_0 is the wave vector in air, ε_r'' is the imaginary part of the relative permittivity, E_r is the normalized electric field intensity, V is the volume of the Si core, I_0 is the solar incident light intensity, and P_{abs} describes the wavelength-dependent absorption mode profile calculated from Poynting theorem, which can be expressed as [33,43-45]

$$P_{abs} = \frac{1}{2} \omega \varepsilon'' |E|^2 \tag{3}$$

$$I_0 = \frac{1}{2} c \varepsilon_0 |E_0|^2 \tag{4}$$

$$\varepsilon_r'' = \varepsilon''/\varepsilon_0 = 2nk \, , E_r = E/E_0 \tag{5}$$

where ω, c, and E_0 is the angular frequency, the speed of light and the electric field intensity of the solar incident light; ε_0 and ε'' are the permittivities in air, and the imaginary part of the permittivity of Si; n and k are the real and imaginary part of the complex refractive index of Si (i.e., $m=n+ik$, $n^2=\varepsilon_r=\varepsilon_r' + i\varepsilon_r''$); E is the electric field intensity in the Si core, respectively.

2.2.2. The electron generation rate

With the assumption that each photon absorbed with the Si core has a contribution to the photocurrent, the spatially dependent electron generation rate is readily calculated by [46,47]

$$G = \int_{300}^{1100} \frac{P_{abs}}{\hbar\omega} d\lambda = \int_{300}^{1100} \frac{\varepsilon'' |E|^2}{2\hbar} d\lambda \tag{6}$$

where $\hbar$ is the reduced Planck's constant.

2.2.3. The photocurrent density

To evaluate the light-harvesting capability as single NW solar cells, we can calculate the photocurrent density J_{ph} by assuming that all generated electron-hole pairs are collected [16,47]:

$$J_{ph} = \frac{q}{C_{geo}} \int_V G dV = q \int_{300}^{1100} \Gamma(\lambda) Q_{abs}(\lambda) d\lambda \tag{7}$$

where q is the element charge, Γ is the solar incident photon flux density.

2.2.4. The photocurrent enhancement factor (PEF)

To evaluate the enhancement of photocurrent of the DSNW, we calculate the photocurrent enhancement factor (PEF) using the relation:

Preprints (www.preprints.org) | NOT PEER-REVIEWED | Posted: 11 August 2020 doi:10.20944/preprints202008.0258.v1

$$\mathrm{PEF}=\left(J_{\mathrm{ph,DSNW}}-J_{\mathrm{ph,rNW}}\right)/J_{\mathrm{ph,rNW}} \tag{8}$$

where $J_{ph,DSNW}$ and $J_{ph,rNW}$ are the photocurrent density for the DSNW and reference NWs (BNW, OSNW, and ISNW), respectively.

Finally, it is important to stress that the unpolarized illumination (i.e., sunlight) is regarded as the average of transverse electric (TE, electric field normal to the NW axis) and transverse magnetic (TM, magnetic field normal to the NW axis) illumination [20,34,35].

$$Q_{\mathrm{abs}}=\left(Q_{\mathrm{abs}}^{\mathrm{TE}}+Q_{\mathrm{abs}}^{\mathrm{TM}}\right)/2 \tag{9}$$

$$J_{\mathrm{ph}}=\left(J_{\mathrm{ph}}^{\mathrm{TE}}+J_{\mathrm{ph}}^{\mathrm{TM}}\right)/2 \tag{10}$$

3. Results and Discussion

3.1. The absorption mechanism

To understand the absorption mechanisms responsible for the improved light-harvesting performance of the DSNW, we investigate the photocurrent density (J_{ph}), the absorption efficiency (Q_{abs}), the absorption mode profile (P_{abs}), and the electron generation rate (G), respectively. Note here that r=100 nm, t=180 nm, i.e., R=r+t=180 nm, t_2=0→180 nm, where t=0, t_2=0, and t_2=180 nm denote the cases of the BNW, OSNW, and ISNW, respectively; m_3 is the complex refractive index of the Si core, m_2=2.0, m_1=1.5, and m_0=1.0, as shown in the insets of Figure 1.

3.1.1. The photocurrent density (J_{ph})

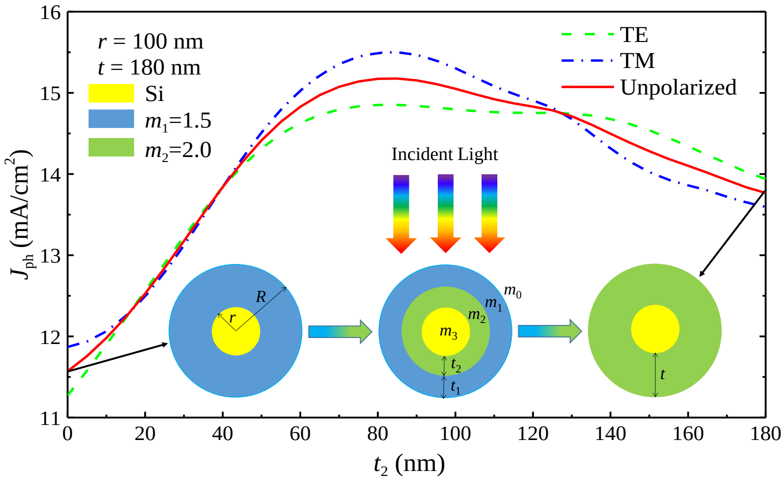

Figure 1. J_{ph} versus t_2 of the DSNW for TE, TM, and unpolarized light illumination. The insets are the cross-sectional views of the OSNW (left), DSNW (middle), and ISNW (right), where J_{ph} is the photocurrent density; t_1, t_2, t=t_1+t_2=180 nm, r=100 nm, and R=r+t=280 nm are the outer shell thickness, inner shell thickness, total shell thickness, core radius, and total radius; m_3, m_2, m_1, and m_0 are the complex refractive indices of the Si core, inner shell, outer shell, and air, respectively.

To evaluate the light-harvesting performance of the DSNW, we first study the effect of the inner shell thickness on the photocurrent density. In Figure 1, we show t_2-dependent J_{ph} under normally-incident TE, TM, and unpolarized light illumination, which is obtained by Equation (7). It is observed that J_{ph} increases rapidly first when initially increasing t_2, reaches a peak at t_2=85 nm, and then decreases when continuing to increase t_2. More importantly, J_{ph} of the DSNWis always bigger than that of the OSNW as long as the inner shell is adopted and higher than that of the ISNW in a broad range of t_2>40 nm. For a direct comparison, we list the J_{ph} values of the considered BNW, OSNW, ISNW, and DSNW configurations under TE, TM, and unpolarized illumination, as shown in Table 1. The maximum J_{ph} values for TE and TM light are 14.85 and 15.50 mA/cm^2, respectively. The unpolarized light illumination (i.e., sunlight), the maximum J_{ph} reaches 15.18 mA/cm^2, which is 96.6%, 31.2%, and 10.2% higher than that of the BNW (7.72 mA/cm^2), OSNW (11.57 mA/cm^2), and ISNW (13.77 mA/cm^2), respectively. It is found that this photocurrent enhancement is mainly ascribed to the improvement of J_{ph} under any polarized situations (especially TM light), indicating the potential of the DSNW in improving the light absorption of single NWs.

Table 1. Photocurrent densities (in mA/cm^2) of the four typical configurations (in nm) of the BNW, OSNW, ISNW, and DSNW under TE, TM, and unpolarized light illumination.

Photocurrent	Configuration	J_{ph}^{TE}	J_{ph}^{TM}	J_{ph}
BNW	r=100, t_2=0, t=0	7.24	8.20	7.72
OSNW	r=100, t_2=0, t=180	11.27	11.87	11.57
ISNW	r=100, t_2=180, t=180	13.94	13.59	13.77
DSNW	r=100, t_2=85, t=180	14.85	15.50	15.18

3.1.2. The absorption efficiency (Q_{abs})

To understand the physical mechanisms of the improved photocurrent, we then examine the absorption spectra of the DSNW. In Figure 2a,b, we present 2D maps of λ-dependent Q_{abs} as a function of t_2 under TE and TM light illumination, which is given by Equation (1). It is clear that dual-shell design leads to full-band absorption enhancement compared to the OSNW, and almost full-band (except several narrow peaks) absorption enhancement compared to the ISNW under both TE and TM light illumination (especially in the off-resonant region), as discussed later. Moreover, J_{ph} periodically changes with increasing t_2 for $\lambda<\lambda_{c1}$ (~430 nm), Q_{abs} reaches the maximum absorption near t_2=50 nm and t_2=130 nm for the first ($t_2<t_{2c}$~90 nm) and second ($t_2>t_{2c}$)) period, respectively. Note that the excellent absorption can be obtained in the range of 40<t_2<60 nm and 110<t_2<140 nm for $\lambda<\lambda_{c1}$. In contrast, Q_{abs} reaches the maximum absorption near t_2=50 nm for $\lambda_{c1}<\lambda<\lambda_{c2}$ (~525 nm), i.e., the superior absorption can be obtained in the range of 60<t_2<120 nm for $\lambda_{c1}<\lambda<\lambda_{c2}$. Besides, Q_{abs} appears to be comparable for $\lambda>\lambda_{c2}$ due to the trade-off between the suppression in the resonant wavelengths and the enhancement in the off-resonant wavelengths, resulting in no contribution to the photocurrent enhancement. It should be noted that t_{2c} is the characteristic inner thickness that denotes the boundary for different absorption periods, and λ_{c1} and λ_{c2} are the characteristic wavelengths that denote the boundaries for different absorption properties, respectively. Therefore, the photocurrent enhancement of the DSNW with t_2<60 nm and t_2>120 nm is attributed to the improved absorption for $\lambda<\lambda_{c1}$, while that of the DSNW with 60<t_2<120 nm is mainly attributed to the improved absorption for $\lambda_{c1}<\lambda<\lambda_{c2}$, which is due to the fact that there is a much higher solar radiation in the range of $\lambda_{c1}<\lambda<\lambda_{c2}$ than $\lambda<\lambda_{c1}$, leading to a more significant contribution to the photocurrent according to Equation (7).

To quantitatively characterize the absorption enhancement of the DSNW, we also examine the absorption spectra corresponding to the optimal J_{ph} in Figure 1. In Figure 2c,d, we show λ-dependent Q_{abs} of the DSNW with t_2=85 nm for TE and TM light, where the results of the BNW, OSNW, and ISNW are also included for comparison. It is shown that Q_{abs} of the DSNW is much higher than that of the BNW and OSNW in the range of $\lambda<\lambda_{c2}$ and that of the ISNW in the range of $\lambda<\lambda_{c2}$ (except for several narrow peaks, i.e., λ=470 for TE light) for both TE and TM light, resulting in a significant photocurrent enhancement. In contrast, although Q_{abs} of the DSNW is weaker at the resonant wavelengths, higher at the off-resonant wavelengths than that of the other three NW structures for $\lambda>\lambda_{c2}$, leading to a similar contribution to the photocurrent, as discussed above. It is worth noting that Q_{abs} can be substantially enhanced at the off-resonance wavelengths over the whole wavelength range for both TE and TM light, especially for TM light (e.g., near λ=470 nm), which results in the more prominent photocurrent enhancement for TM than TE light. It should also be noted that the match between the absorption efficiency and the solar spectrum becomes another essential factor in evaluating the photocurrent according to Equation (7). For instance, although Q_{abs} of the DSNW for

Preprints (www.preprints.org) | NOT PEER-REVIEWED | Posted: 11 August 2020 doi:10.20944/preprints202008.0258.v1

TE light is much higher than that for TM light in the range of $\lambda<\lambda_{c1}$, solar radiation is much lower, which leads to a less photocurrent enhancement, while Q_{abs} for TM light is much higher than that for TM light in the range of 450<λ<650 nm (except the narrow range of 490<λ<505 nm), as shown in the inset of Figure 2d, and solar radiation is much higher at the same time, which results in a more significant contribution to the photocurrent.

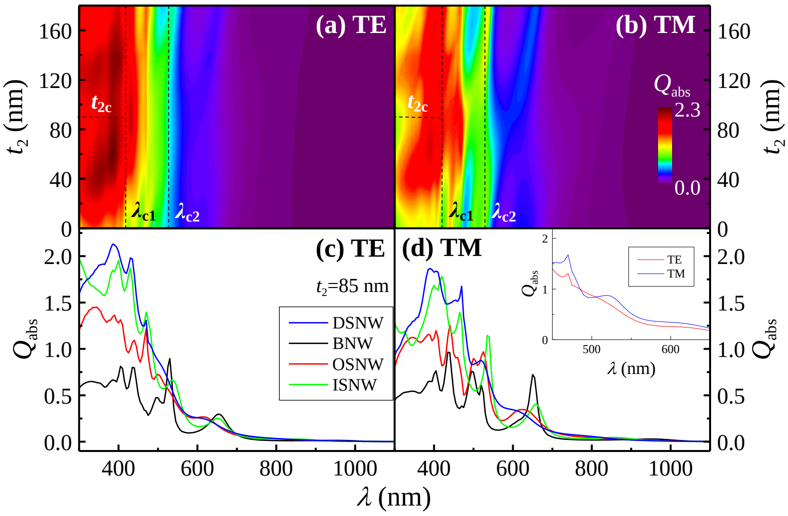

Figure 2. Q_{abs} versus λ and t_2 of the DSNW for (a) TE and (b) TM light illumination; Q_{abs} versus λ of the DSNW (t_2=85 nm) under (c) TE and (d) TM light illumination, together with the BNW (t=0), OSNW (t_2=0), and ISNW (t_2=180 nm) as references. The inset in (d): Q_{abs} versus λ (450-650 nm) for TE and TM light, where Q_{abs}, λ, and t_2 are the absorption efficiency, the wavelength of the incident light, and the inner shell thickness, respectively.

3.1.3. The absorption mode profile (P_{abs})

The absorption behavior presented above can be well described by the absorption mode profiles calculated by Equation (3) [20,22,24,44,46]. In Figure 3, we examine the normalized absorption mode profiles inside the Si core corresponding to the wavelengths in Figure 2c under TE and TM light illumination (these profiles from left to right columns are related to the evolution of the structure from BNW to OSNW, and then to ISNW, and finally to DSNW). Figure 3a,c show the off-resonance absorption profiles for TE and TM light, while Figure 3b,d show the corresponding resonant absorption profiles. It is observed that the absorption enhancement is attributed to the excitation of the leaky mode resonances (LMRs), likewise in BNW[15,16], which can capture light by multiple total internal reflections at the Si core/inner shell interface when the wavelength of the incident light matches one of the LMRs supported by the Si core. The LMRs can be noted as TM_{ml} or TE_{ml}, where m and l are the azimuthal mode number and the radial order of the resonances, respectively. Figure 3b,d show that the resonant absorption mode profiles of DSNW are different from that of BNW, similar to that of the INSW due to the fact that the LMRs occur at the Si core/inner shell interface. Specifically, the modes of the BNW, OSNW, ISNW, and DSNW are TE_{12}, TE_{31}, TE_{31}, and TE_{31} at λ= 495, 470, 470, and 470 nm for TE light, and TM_{12}, TM_{41}, TM_{12}, and TM_{12} at λ= 495, 500, 465, and 470 nm, respectively. The absorption is indeed enhanced compared to the BNW and OSNW for both TE and TM light, and slightly suppressed for TE light and enhanced for TM light compared to the ISNW. Figure 3a,c show that the off-resonant absorption mode profiles of the DSNW exhibit a transition mode referred to the LMRs, such transition modes are very close to the corresponding LMRs that is attributed to the fact that the graded dual shells make the incident light couple into the Si core, leading to a more significant absorption enhancement compared to the other three NWs.

The absorption behavior presented above can also be well understood by employing the Fano resonance [48] that occurs when a discrete localized state is coupled with a continuum of state. In other words, Fano resonance is an asymmetric resonance due to the interference between a narrow resonance (e.g., localized reemitted light, LMRs) and a continuum or a broad resonance (e.g.,

Preprints (www.preprints.org) | NOT PEER-REVIEWED | Posted: 11 August 2020 doi:10.20944/preprints202008.0258.v1

sunlight), which has been intensively investigated in nanostructures [49-51]. For stronger LMRs ($\lambda > \lambda_{c2}$) of the BNW, as shown in Figure 2, both the absorption at resonant and off-resonant wavelengths is greatly enhanced due to the constructive interferences between the weaker LMRs (or transition modes) of the Si core and incident light. However, for stronger LMRs ($\lambda > \lambda_{c2}$) of the BNW, the absorption at the resonant wavelengths is suppressed due to the destructive interference between the stronger LMRs of the Si core and incident light. In contrast, the absorption at the off-resonant wavelengths is greatly enhanced due to the constructive interferences between the weaker transition modes of the Si core and incident light from the graded dual shells. In a word, the off-resonant or weaker resonant absorption is dramatically enhanced. In comparison, the stronger resonant absorption is suppressed compared to the other three NWs, which is ascribed to the constructive or destructive interferences between the reemitted light of the leaky mode resonances of the Si core and the nanofocusing light from the graded dual shells at the core/inner shell interface.

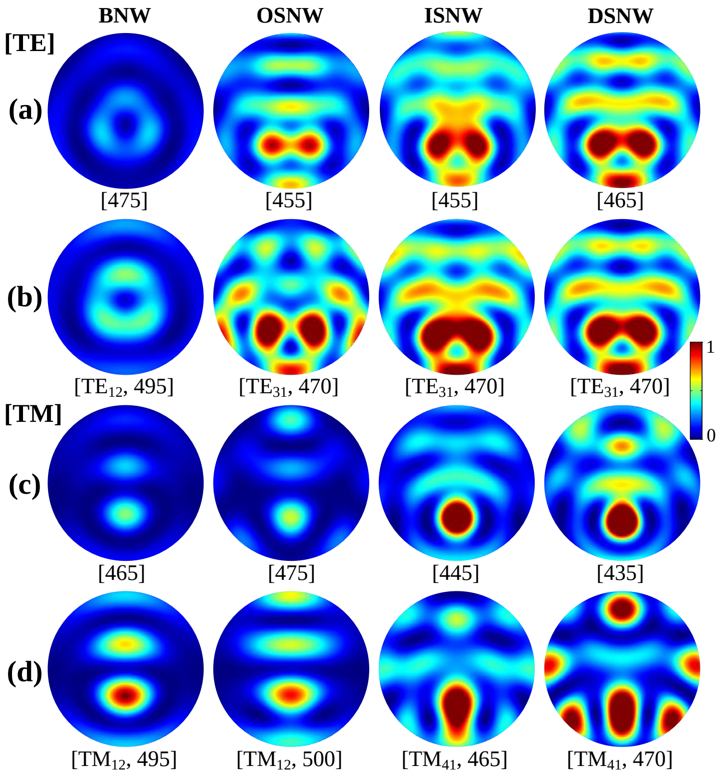

Figure 3. The representative normalized absorption mode profiles inside the Si core corresponding to the wavelengths in Figure 2c,d [from left to right columns are associated with the BNW, OSNW, ISNW, and DSNW, respectively]: (a,b) for TE and (c,d) for TM light illumination; (a,c) for off-resonant and (b,d) for on-resonant wavelengths.

3.1.4. The generation rate profile (*G*)

To further confirm the physical origins discussed above, we show the electron generation rate obtained Equation (6). In Figure 4, we present the normalized generation rate profiles for TE and TM polarized light, respectively. Figure 4a shows that the absorption of the DSNW for TE light is much stronger than that of the BNW and OSNW and that of almost all the regions of the ISNW [evidently enhanced in the regions labeled by circles (see Figure 4a) and slightly decreased in the region labeled by the square (see Figure 4a)]. Figure 4b shows that the absorption of the DSNW for TM light is also much stronger than that of the BNW and OSNW and that of almost all the regions of the ISNW [evidently enhanced in the regions by labeled by triangles (see Figure 4b)]. These results reveal that this enhancement arises mainly from the off-resonant absorption due to the improved coupling between the reemitted light of the leaky mode resonances of the Si core and the nanofocusing light from the graded dual shells. More importantly, the generation rate profiles of the DSNW for both TE and TM light have similar patterns with that of the other three NWs, again indicating that the absorption enhancement is mainly attributed to the LMRs, likewise in the BNWs.

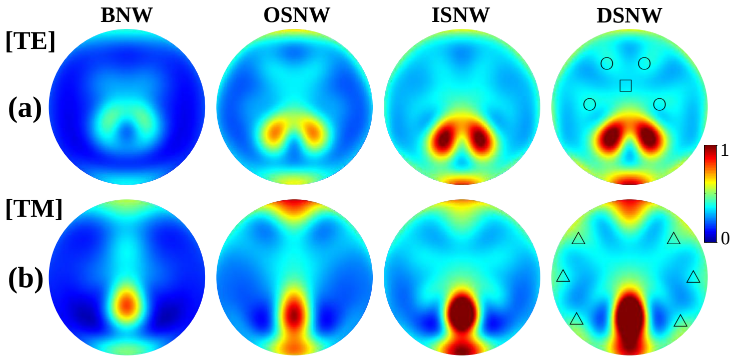

Figure 4. The normalized generation rate profiles of the DSNW for (a) TE and (b) TM light, together with the BNW, OSNW, and ISNW for comparison.

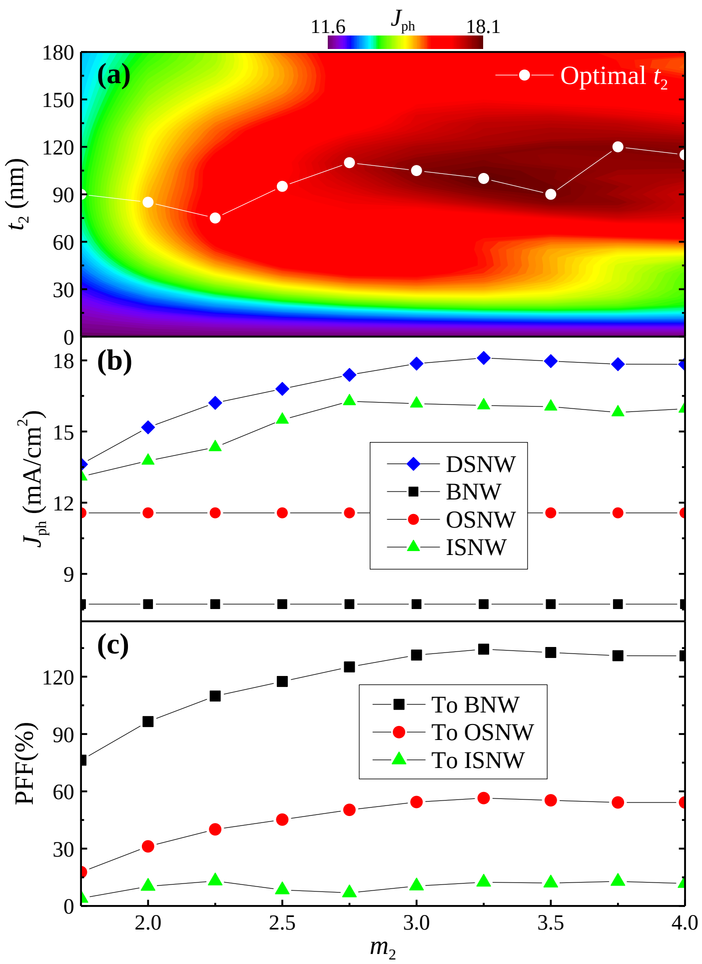

Figure 5. (a) J_{ph} versus t_2 and m_2 of the DSNW. The white dashed line represents the position of the maximized J_{ph} at various m_2 values. (b) J_{ph} versus m_2 of the DSNW, corresponding to the optimal t_2. Also, J_{ph} of the BNW, OSNW, and ISNW are included for comparison. (c) The photocurrent enhancement factors (PEFs) versus m_2 of the DSNW compared to the BNW, OSNW, and ISNW, respectively.

3.2. The optimization of the light-harvesting performance

To evaluate and optimize the light-trapping performance of the DSNW for photovoltaic applications, we now investigate the effect of both the shell thickness and complex refractive index

Preprints (www.preprints.org) | NOT PEER-REVIEWED | Posted: 11 August 2020 doi:10.20944/preprints202008.0258.v1

on the photocurrent density calculated using Equation (7). Note that the structural details of the DSNW are consistent with that shown in the insets of Figure 1, except for m_2. In Figure 4a, we show 2D J_{ph} as a function of t_2 and m_2 of the DSNW and the optimal t_2 as a function of m_2. J_{ph} sharply increases with increasing t_2 at a fixed m_2, reaches its maximum, and then decreases when continuing to increase t_2. More importantly, J_{ph} of the DSNW is always much larger than that of the OSNW at any t_2 values and higher than that of the ISNW in a broad range of t_2>40 nm when m_2<3.5 and t_2>60 nm when 3.5<m_2<4.0. It is observed that the maxima of J_{ph} can be obtained when 3.0<m_2<3.5 and 90<t_2<110 nm. In Figure 5b, we show m_2-dependent J_{ph} of the DSNW (corresponding to the optimal t_2 in Figure 5a), together with that of the BNW, OSNW, and ISNW for comparison. Also, in Figure 5c, we show the photocurrent enhancement factors (PEFs) defined by Equation (8). It is readily observed that J_{ph} of the DSNW is much larger than the other three NWs. In particular, the max J_{ph} = 18.10 mA/cm^2 at m_2=3.25 and t_2=100 nm, which is 134.4%, 56.4%, and 12.4% much larger than that of the BNW (7.72 mA/cm^2), OSNW (11.57 mA/cm^2), and OSNW (16.10 mA/cm^2), respectively.

4. Conclusions

In summary, we proposed a single NW by coating dual dielectric shells. The influence of the thickness and complex refractive index of the DSNWs on the light absorption for photovoltaic applications are investigated. It is found that the size and material of the inner shell can lead to significantly improved off-resonant absorption. The examination of the spatial profiles of the absorption mode and generation rate reveals that the enhancement effect is the result of constructive interference under the improved coupling between the reemitted light of the leaky mode resonances of the Si core and the nanofocusing light from the graded dual shells. The results show that the photocurrent density can be enhanced by 134.4%, 56.4%, and 12.4% in comparison with that of the BNW, OSNW, and ISNW, respectively. Therefore, such a dual shell coated structure can be applied to various semiconductors to improve the off-resonant absorption and provides an effective way to achieve high-efficiency single NW solar cells.

Author Contributions: Conceptualization, W.L. and Y.Y.; methodology, W.L., X.G. and S.X.; software, W.L., H.Y. and D.W; investigation, W.L., D.W, H.Y., Y.W. and L.B.; writing—original draft preparation, W.L.; writing—review and editing, W.L., X.G., S.X., Q.W., L.Z., X.Z., X.W. and Y.Y. All authors have read and agreed to the published version of the manuscript.

Funding: This research was funded by the National Natural Science Foundation of China (Grant No. 61404057, 51801068, and 11875284), Key disciplines Fund for Optical Engineering in Henan Province (Grant No. 2018119), and Key Youth Teacher of Universities in Henan Province (Grant No. 2016GGJS-145).

Acknowledgments: We would also like to thank the support from China Scholarship Council (Grant No. 201902720047) and the Construction of Master's Program on Energy and Power Engineering at Huanghuai University.

Conflicts of Interest: The authors declare no conflict of interest.

References

1. Tian, B.; Zheng, X.; Kempa, T.J.; Fang, Y.; Yu, N.; Yu, G.; Huang, J.; Lieber, C.M. Coaxial silicon nanowires as solar cells and nanoelectronic power sources. *Nature* **2007**, *449*, 885-889, Doi:10.1038/nature06181.
2. Nehra, M.; Dilbaghi, N.; Marrazza, G.; Kaushik, A.; Abolhassani, R.; Mishra, Y.K.; Kim, K.H.; Kumar, S. 1D semiconductor nanowires for energy conversion, harvesting and storage applications. *Nano Energy* **2020**, *76*, 104991, Doi:10.1016/j.nanoen.2020.104991.
3. Li, Z.; Tan, H.H.; Jagadish, C.; Fu, L. III–V Semiconductor Single Nanowire Solar Cells: A Review. *Adv. Mater. Technol.* **2018**, *3*, 1800005, Doi:10.1002/admt.201800005.
4. Kempa, T.J.; Day, R.W.; Kim, S.-K.; Park, H.-G.; Lieber, C.M. Semiconductor nanowires: a platform for exploring limits and concepts for nano-enabled solar cells. *Energy Environ. Sci.* **2013**, *6*, 719-733, Doi:10.1039/C3EE24182C.

5. Christesen, J.D.; Zhang, X.; Pinion, C.W.; Celano, T.A.; Flynn, C.J.; Cahoon, J.F. Design principles for photovoltaic devices based on Si nanowires with axial or radial p–n junctions. *Nano Lett.* **2012**, *12*, 6024-6029, Doi:10.1021/nl303610m.
6. Zhan, Y.; Li, X.; Li, Y. Numerical Simulation of Light-Trapping and Photoelectric Conversion in Single Nanowire Silicon Solar Cells. *IEEE J. Sel. Top. Quantum Electron.* **2013**, *19*, 1-8, Doi:10.1109/jstqe.2013.2246771.
7. Tian, B.; Kempa, T.J.; Lieber, C.M. Single nanowire photovoltaics. *Chem. Soc. Rev.* **2009**, *38*, 16-24, Doi:10.1039/B718703N.
8. Tang, J.; Huo, Z.; Brittman, S.; Gao, H.; Yang, P. Solution-processed core-shell nanowires for efficient photovoltaic cells. *Nat. Nanotechnol.* **2011**, *6*, 568-572, Doi:10.1038/NNANO.2011.139.
9. Holm, J.V.; Jørgensen, H.I.; Krogstrup, P.; Nygård, J.; Liu, H.; Aagesen, M. Surface-passivated GaAsP single-nanowire solar cells exceeding 10% efficiency grown on silicon. *Nat. Commun.* **2013**, *4*, 1498, Doi:10.1038/ncomms2510.
10. Yuan, X.; Chen, X.; Yan, X.; Wei, W.; Zhang, Y.; Zhang, X. Absorption-Enhanced Ultra-Thin Solar Cells Based on Horizontally Aligned p–i–n Nanowire Arrays. *Nanomaterials* **2020**, *10*, 1111, Doi:10.3390/nano10061111.
11. Chen, W.; Roca i Cabarrocas, P. Rational design of nanowire solar cells: from single nanowire to nanowire arrays. *Nanotechnology* **2019**, *30*, 194002, Doi:10.1088/1361-6528/aaff8d.
12. Otnes, G.; Barrigón, E.; Sundvall, C.; Svensson, K.E.; Heurlin, M.; Siefer, G.; Samuelson, L.; Åberg, I.; Borgström, M.T. Understanding InP Nanowire Array Solar Cell Performance by Nanoprobe-Enabled Single Nanowire Measurements. *Nano Lett.* **2018**, *18*, 3038-3046, Doi:10.1021/acs.nanolett.8b00494.
13. Song, K.-D.; Kempa, T.J.; Park, H.-G.; Kim, S.-K. Laterally assembled nanowires for ultrathin broadband solar absorbers. *Opt. Express* **2014**, *22*, A992-A1000, Doi:10.1364/OE.22.00A992.
14. Zhang, X.; Pinion, C.W.; Christesen, J.D.; Flynn, C.J.; Celano, T.A.; Cahoon, J.F. Horizontal Silicon Nanowires With Radial p-n Junctions: A Platform for Unconventional Solar Cells. *J. Phys. Chem. Lett.* **2013**, *4*, 2002–2009, Doi:10.1021/jz400533.
15. Cao, L.; White, J.S.; Park, J.-S.; Schuller, J.A.; Clemens, B.M.; Brongersma, M.L. Engineering light absorption in semiconductor nanowire devices. *Nat. Mater.* **2009**, *8*, 643-647, Doi:10.1038/nmat2477.
16. Cao, L.; Fan, P.; Vasudev, A.P.; White, J.S.; Yu, Z.; Cai, W.; Schuller, J.A.; Fan, S.; Brongersma, M.L. Semiconductor Nanowire Optical Antenna Solar Absorbers. *Nano Lett.* **2010**, *10*, 439-445, Doi:10.1021/nl9036627.
17. Brönstrup, G.; Jahr, N.; Leiterer, C.; Csáki, A.; Fritzsche, W.; Christiansen, S. Optical properties of individual silicon nanowires for photonic devices. *ACS Nano* **2010**, *4*, 7113-7122, Doi:10.1021/nn101076t.
18. Kim, S.; Cahoon, J.F. Geometric Nanophotonics: Light Management in Single Nanowires through Morphology. *Acc. Chem. Res.* **2019**, *52*, 3511-3520, Doi:10.1021/acs.accounts.9b00515.
19. Choi, J.S.; Kim, K.-H.; No, Y.-S. Spatially localized wavelength-selective absorption in morphology-modulated semiconductor nanowires. *Opt. Express* **2017**, *25*, 22750-22759, Doi:10.1364/OE.25.022750.
20. Zhang, C.; Yang, Z.; Wu, K.; Li, X. Design of asymmetric nanovoid resonator for silicon-based single-nanowire solar absorbers. *Nano Energy* **2016**, *27*, 611-618, Doi:10.1016/j.nanoen.2016.08.017.
21. Yang, Z.; Cao, G.; Shang, A.; Lei, D.Y.; Zhang, C.; Gao, P.; Ye, J.; Li, X. Enhanced Photoelectrical Response of Hydrogenated Amorphous Silicon Single-Nanowire Solar Cells by Front-Opening Crescent Design. *Nanoscale Res. Lett.* **2016**, *11*, 233, Doi:10.1186/s11671-016-1447-0.
22. Yang, Z.; Li, X.; Lei, D.Y.; Shang, A.; Wu, S. Omnidirectional absorption enhancement of symmetry-broken crescent-deformed single-nanowire photovoltaic cells. *Nano Energy* **2015**, *13*, 9-17, Doi:10.1016/j.nanoen.2015.02.007.
23. Luo, S.; Yu, W.B.; He, Y.; Ouyang, G. Size-dependent optical absorption modulation of Si/Ge and Ge/Si core/shell nanowires with different cross-sectional geometries. *Nanotechnology* **2015**, *26*, 085702, Doi:10.1088/0957-4484/26/8/085702.
24. Kim, S.-K.; Song, K.-D.; Kempa, T.J.; Day, R.W.; Lieber, C.M.; Park, H.-G. Design of Nanowire Optical Cavities as Efficient Photon Absorbers. *ACS Nano* **2014**, *8*, 3707–3714, Doi:10.1021/nn5003776.
25. Kim, S.-K.; Day, R.W.; Cahoon, J.F.; Kempa, T.J.; Song, K.-D.; Park, H.-G.; Lieber, C.M. Tuning Light Absorption in Core/Shell Silicon Nanowire Photovoltaic Devices through Morphological Design. *Nano Lett.* **2012**, *12*, 4971-4976, Doi:10.1021/nl302578z.

26. Kempa, T.J.; Cahoon, J.F.; Kim, S.-K.; Day, R.W.; Bell, D.C.; Park, H.-G.; Lieber, C.M. Coaxial multishell nanowires with high-quality electronic interfaces and tunable optical cavities for ultrathin photovoltaics. *P. Natl. Acad. Sci. USA* **2012**, *109*, 1407-1412, Doi:10.1073/pnas.1120415109.
27. Liu, W.F.; Oh, J.I.; Shen, W.Z. Light Trapping in Single Coaxial Nanowires for Photovoltaic Applications. *IEEE Electron Device Lett.* **2011**, *32*, 45-47, Doi:10.1109/LED.2010.2086428.
28. Liu, W.F.; Oh, J.I.; Shen, W.Z. Light absorption mechanism in single c-Si (core)/a-Si (shell) coaxial nanowires. *Nanotechnology* **2011**, *22*, 125705, Doi:10.1088/0957-4484/22/12/125705.
29. Zhong, Z.; Li, Z.; Gao, Q.; Li, Z.; Peng, K.; Li, L.; Mokkapati, S.; Vora, K.; Wu, J.; Zhang, G., et al. Efficiency enhancement of axial junction InP single nanowire solar cells by dielectric coating. *Nano Energy* **2016**, *28*, 106-114, Doi:10.1016/j.nanoen.2016.08.032.
30. Solanki, A.; Gentile, P.; Boutami, S.; Calvo, V.; Pauc, N. Dielectric Coating-Induced Absorption Enhancement in Si Nanowire Junctions. *Adv. Opt. Mater.* **2015**, *3*, 120-128, Doi:10.1002/adom.201400334.
31. Kim, S.-K.; Zhang, X.; Hill, D.J.; Song, K.-D.; Park, J.-S.; Park, H.-G.; Cahoon, J.F. Doubling Absorption in Nanowire Solar Cells with Dielectric Shell Optical Antennas. *Nano Lett.* **2015**, *15*, 753-758, Doi:10.1021/nl504462e.
32. Yu, Y.; Ferry, V.E.; Alivisatos, A.P.; Cao, L. Dielectric Core–Shell Optical Antennas for Strong Solar Absorption Enhancement. *Nano Lett.* **2012**, *12*, 3674-3681, Doi:10.1021/nl301435.
33. Li, X.; Zhan, Y.; Wang, C. Broadband enhancement of coaxial heterogeneous gallium arsenide single-nanowire solar cells. *Prog. Photovolt. Res. Appl.* **2015**, *23*, 628-636, Doi:10.1002/pip.2480.
34. Zhang, C.; Yang, Z.; Shang, A.; Wu, S.; Zhan, Y.; Li, X. Improved optical absorption of silicon single-nanowire solar cells by off-axial core/shell design. *Nano Energy* **2015**, *17*, 233-240, Doi:10.1016/j.nanoen.2015.08.017.
35. Zhou, J.; Zhang, Z.; Wu, Y.; Xia, Z.; Qin, X. Significantly enhanced coupling to half-space irradiation using a partially capped nanowire for solar cells. *Nano Energy* **2018**, *45*, 61-67, Doi:10.1016/j.nanoen.2017.12.027.
36. Saylan, S.; Milakovich, T.; Hadi, S.A.; Nayfeh, A.; Fitzgerald, E.A.; Dahlem, M.S. Multilayer antireflection coating design for $GaAs_{0.69}P_{0.31}$/Si dual-junction solar cells. *Sol. Energy* **2015**, *122*, 76-86, Doi:10.1016/j.solener.2015.07.049.
37. Tsai, M.-T.; Yang, Z.-P.; Jing, T.-S.; Hsieh, H.-H.; Yao, Y.-C.; Lin, T.-Y.; Chen, Y.-F.; Lee, Y.-J. Achieving graded refractive index by use of ZnO nanorods/TiO_2 layer to enhance omnidirectional photovoltaic performances of InGaP/GaAs/Ge triple-junction solar cells. *Sol. Energy Mater. Sol. Cells* **2015**, *136*, 17-24, Doi:10.1016/j.solmat.2014.12.019.
38. Yeh, L.K.; Lai, K.Y.; Lin, G.J.; Fu, P.H.; Chang, H.C.; Lin, C.A.; He Jr, H. Giant efficiency enhancement of GaAs solar cells with graded antireflection layers based on syringelike ZnO nanorod arrays. *Adv. Energy Mater.* **2011**, *1*, 506-510, Doi:10.1002/aenm.201100025.
39. Palik, E.D. *Handbook of Optical Constants of Solids*; Academic Press: London, UK, 1985; Vol. 1, pp. 547-552.
40. Kane, Y. Numerical Solution of Initial Boundary Value Problems Involving Maxwell's Equations in Isotropic Media. *IEEE Trans. Antennas Propag.* **1966**, *14*, 302-307, Doi:10.1109/TAP.1966.1138693.
41. Taflove, A.; Hagness, S.C. *Computational Electrodynamics: The Finite-Difference Time-Domain Method*, 3rd ed.; Artech House: Norwood, MA, USA, 2005.
42. Ee, H.S.; Song, K.D.; Kim, S.K.; Park, H.G. Finite-Difference Time-Domain Algorithm for Quantifying Light Absorption in Silicon Nanowires. *Isr. J. Chem.* **2012**, *52*, 1027-1036, Doi:10.1002/ijch.201200061.
43. Bohren, C.F.; Huffman, D.R. *Absorption and Scattering of Light by Small Particles* John Wiley & Sons, Inc.: New York, USA, 1998; pp. 57-81, 202-204.
44. Zhou, L.; Yu, X.; Zhu, J. Metal-Core/Semiconductor-Shell Nanocones for Broadband Solar Absorption Enhancement. *Nano Lett.* **2014**, *14*, 1093-1098, Doi:10.1021/nl500008y.
45. Mann, S.A.; Garnett, E.C. Extreme Light Absorption in Thin Semiconductor Films Wrapped around Metal Nanowires. *Nano Lett.* **2013**, *13*, 3173-3178, Doi:10.1021/nl401179h.
46. Ferry, V.E.; Polman, A.; Atwater, H.A. Modeling light trapping in nanostructured solar cells. *ACS Nano* **2011**, *5*, 10055-10064, Doi:10.1021/nn203906t.
47. Munday, J.N.; Atwater, H.A. Large integrated absorption enhancement in plasmonic solar cells by combining metallic gratings and antireflection coatings. *Nano Lett.* **2010**, *11*, 2195-2201, Doi:10.1021/nl101875t.
48. Fano, U. Effects of configuration interaction on intensities and phase shifts. *Phys. Rev.* **1961**, *124*, 1866-1878, Doi:10.1103/PhysRev.124.1866.

 doi:10.20944/preprints202008.0258.v1

49. Luk'yanchuk, B.; Zheludev, N.I.; Maier, S.A.; Halas, N.J.; Nordlander, P.; Giessen, H.; Chong, C.T. The Fano resonance in plasmonic nanostructures and metamaterials. *Nat. Mater.* **2010**, *9*, 707-715, Doi:10.1038/nmat2810.
50. Limonov, M.F.; Rybin, M.V.; Poddubny, A.N.; Kivshar, Y.S. Fano resonances in photonics. *Nat. Photonics* **2017**, *11*, 543-554, Doi:10.1038/nphoton.2017.142.
51. Abujetas, D.R.; Mandujano, M.A.G.; Méndez, E.R.; Sánchez-Gil, J.A. High-Contrast Fano Resonances in Single Semiconductor Nanorods. *ACS Photonics* **2017**, *4*, 1814-1821, Doi:10.1021/acsphotonics.7b00395.